J. Fluid Mech. (1968), *vol.* 31, *part* 3, *pp.* 435–448
Printed in Great Britain

Vortex evolution in a round jet

By H. A. BECKER

Department of Chemical Engineering, Queen's University, Kingston, Ontario, Canada

AND T. A. MASSARO

Department of Chemical Engineering, University of California, Berkeley, California

(Received 17 January 1967 and in revised form 9 October 1967)

A study has been made of the varicose instability of an axisymmetrical jet with a velocity distribution radially uniform at the nozzle mouth except for a laminar boundary layer at the wall. The evolutionary phenomena of instability, such as the rolling up of the cylindrical vortex layer into ring vortices, the coalescence of ring vortex pairs, and the eventual disintegration into turbulent eddies, have been investigated as a function of the Reynolds number using smoke photography, stroboscopic observation, and the light-scatter technique.

Emphasis has been placed on the wavelength with maximum growth rate. The jet is highly sensitive to sound and the effects of several types of acoustic excitation, including pure tones, have been determined.

1. Introduction

The acoustic sensitivity of jets has been a subject of scientific curiosity ever since Leconte (1858) noticed the jumping of a coalgas flame-jet in response to certain notes of a violoncello and suggested, 'We must look upon all jets as musically-inclined'. The phenomenon was first known as the 'sensitive flame', but Tyndall shortly showed that combustion is inessential and similar effects may be observed in any gas jet under suitable conditions. Rayleigh introduced stroboscopic illumination (1884) and analysed the instability problem (1879). He recognized (i) varicose instability in which pulsations or waves synchronous with the exciting tone travel along the jet as a succession of symmetrical swellings and contractions, and (ii) sinuous instability in which the waves appear by a rythmic undulation or twisting of the jet.

The present work started during a study of turbulent jet mixing. Under stroboscopic illumination a beautiful spectacle of varicose instability and ring vortex shedding was seen when the nozzle air was marked with smoke. Then the acoustic sensitivity of the jet was noticed and a further investigation ensued. A literature search showed that many of the phenomena had already been observed by Anderson (1955, 1956), and by workers at the Hermann Föttinger Institut in Berlin (Domm, Fabian, Wehrmann & Wille 1955; Wehrmann, Fabian & Wille 1956; Wehrmann & Wille 1957; Schade & Michalke 1962; Wille 1963). The associated theory has also been extensively developed (Rayleigh 1899;

Domm 1956; Batchelor & Gill 1962; Michalke & Schade 1963; Michalke 1964). Our principal contribution in the present paper is therefore to report some detailed observations which our methods (the light scatter technique and photography by sheet illumination) made possible and which should contribute to a clearer understanding of the vortex evolution with Reynolds number and distance from the nozzle.

2. Apparatus and methods

The jet nozzle

Since the nozzle influenced the phenomena, the design is of interest. The ASME standard for short radius nozzles was used, the salient feature of which is the $\frac{4}{3}D$ minor dia. times $2D$ major dia. elliptical fairing followed by a $0{\cdot}6D$ straight run, figure 1(*a*), where D is the throat diameter, here 0·635 cm. The nozzle was smoothly joined to a 2·414 cm inside dia. pipe. The nozzle chamber, figure 1(*b*),

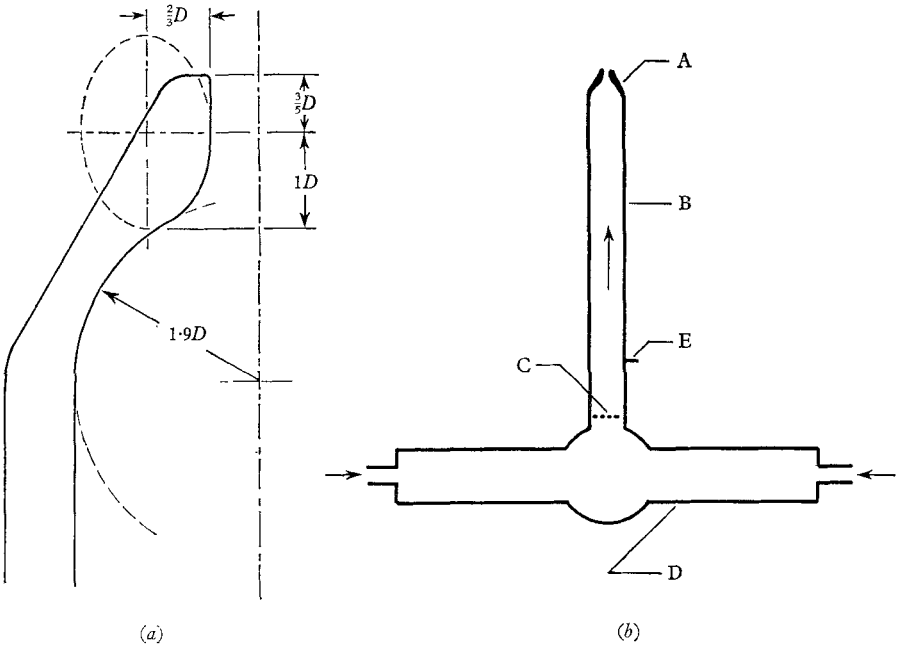

FIGURE 1. (*a*) The nozzle design with elliptical fairing and throat proportions based on ASME specifications (D is the throat diameter). (*b*) The nozzle chamber: A, nozzle; B, 2·414 cm I.D. by 30 cm long pipe; C, screen; D, calming chamber; E, static pressure tap.

was from another investigation but was used without change. Equal streams of air from left and right mingled in the calming chamber D and then flowed up through screen C, through the nozzle pipe B, and finally out through the nozzle A. Roughly speaking, the nozzle pipe and the calming chamber formed a resonator with a total volume of *ca.* 500 cm^3, an aperture area of 0·317 cm^2, and a neck length of *ca.* 1 cm. The resonance frequency calculated from these numbers is *ca.* 110 c/s. The lowest frequency at which the jet exhibited a maximum in acoustic sensitivity was, significantly, 103 ± 3 c/s.

Flow visualization

The nozzle airstream was made visible with an oil condensation smoke.

Acoustic excitation

The jet was subjected to three types of acoustic excitation: (i) *Silence.* The experiments were done after midnight on calm nights to minimize background noise, vibration and drafts. Smoke discharged during runs collected at the ceiling and was exhausted periodically. (ii) *Pure tones.* A loudspeaker driven by an audio-oscillator was played at the jet from about 45° above the nozzle and 50 cm away. The room was otherwise 'silent'. (iii) *Intense noise.* A hood for exhausting the smoke was located in the ceiling above the jet. The exhaust fan was run during these experiments and made a deafening roar.

Vortex shedding frequency

Vortex frequencies up to 2100 vortices/sec were unambiguously measured by stroboscopic observation. At higher frequencies the scattered-light technique (Becker, Hottel & Williams 1967) was used in which, with a photocell and appropriate optics, a signal is generated which is proportional to the instantaneous point concentration of the marking smoke. At the jet edge the smoke concentration in the varicosely unstable region fluctuates between the nozzle value and the ambient (zero). Spectral analysis gives the vortex frequency.

Photography

Two techniques of illuminating the smoke jet were used: (i) general illumination, and (ii) sheet illumination through a slit. The latter gave a view of a longitudinal cross-section about 2 mm thick.

Photographs were made on Polaroid 3000 film using: (i) single-flash exposure, giving the 'instantaneous' view; (ii) time exposure by steady illumination, giving the overall time-average; and (iii) time exposure by stroboscopic illumination synchronized with the vortex frequency, giving a time-average of the determinate aspects of the vortex pattern.

A high-speed movie (3000 frames/sec) was made using intense general illumination (attempts with sheet illumination failed).

3. The nozzle boundary layer

The nozzle velocity profile was flat except for the wall boundary layer. The displacement thickness at efflux, δ, was found by measuring the volumetric rate of discharge Q and the pressure drop through the nozzle. The pressure drop, by Bernoulli's formula, gives the velocity in the potential core, U_0. Then

$$Q = \pi(a-\delta)^2 U_0,$$

where a is the throat radius. The data were correlated by the equation

$$\delta/D = 0{\cdot}9/\sqrt{Re}, \tag{1}$$

where $Re \equiv U_0 D/\nu$ is the nozzle Reynolds number. Substitution of $x \simeq \frac{3}{2}D$ in the Blasius flat-plate formula gives the estimate $\delta/D \simeq 2/\sqrt{Re}$. Since we are dealing with a converging potential flow, the experimental constant, 0·9, is of the right magnitude.

4. Effects of pure acoustic excitation

A marked acoustic selectivity was found at Reynolds numbers below 10,000. The frequencies eliciting minimum response were determined with pure tones from the loudspeaker. The intensity of the exciting tone had no visible effect above a certain level. The observations were therefore made with the intensity set comfortably high on this plateau. At a critical frequency the jet flared near its

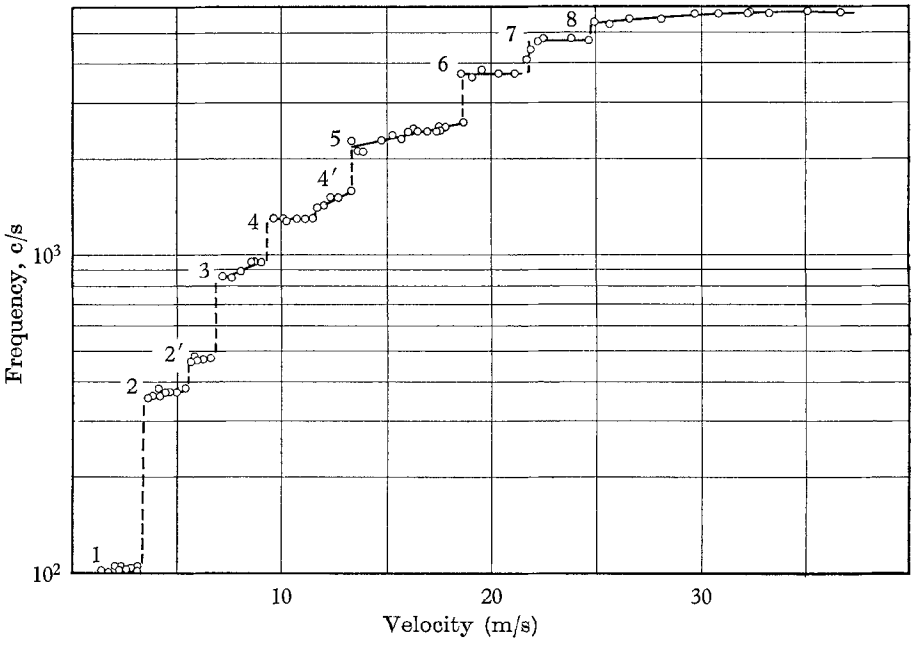

FIGURE 3. The frequency of the pure tone giving maximum excitation of the jet as a function of the nozzle velocity.

root. The initial angle of spread as much as doubled and the points of appearance of ring vortices and of turbulent breakdown moved closer to the nozzle. Maxima were sometimes found at several frequencies, but the dominant frequency was never ambiguous.

The acoustic sensitivity of the jet is illustrated in figure 2, plate 1. Plates 1 (*a*), (*b*) and (*c*) show the jet in 'silence'. The nozzle Reynolds number of 1690 is low and the length for turbulent breakdown correspondingly large. Plate 1(*b*) shows that breakdown occurred by sinuous instability. However, the close-up in (*c*) indicates that the disturbance became sinuous only some distance downstream. This shift is evidently connected with the disappearance of the potential core of the jet about 5 nozzle diameters from the nozzle. Sinuous instability was not observed at Reynolds numbers above 2300. Plates 1 (*d*), (*e*) and (*f*) show the

same jet maximally excited by a pure tone. The instability is now varicose and the waves quickly roll up into ring vortices. Some half-dozen wavelengths from the nozzle, the vortices disintegrate into turbulent eddies.

The variation of the maximal excitation frequency with nozzle velocity was discontinuous, (figure 3). For easy reference the ten resonance régimes have been numbered 1, 2, 2′, 3, 4, 4′, 5, 6, 7 and 8, where 2′ and 4′ are of minor distinction. The characteristics of these régimes are summarized in table 1.

Régime	Range of Re	Frequency (c/s)	Remarks
1	–1450	103	$f_0 = 103$†
2	1450–2300	370	$4(f-f_0) = 1070$
2′	2300–2800	470	$3(f-f_0) = 1100$
3	2800–3800	850–950	$3(f-f_0)/2 = 1200$
4	3800–4750	1300	$-f_0 = 1200$
4′	4750–5500	1400–1600	—
5	5500–7600	2200–2600	$(f-f_0)/2 = 1150$
6	7600–8900	3700	$(f-f_0)/3 = 1200$
7	8900–10000	4700	$(f-f_0)/4 = 1150$
8	10000–	5700	$(f-f_0)/5 = 1120$

† This appears to be the first resonance frequency of the nozzle chamber; calculation gives 110 c/s.

TABLE 1. Characteristics of the resonance régimes.

From the viewpoint of instability theory the most interesting aspect of the results is the general trend of the resonance frequencies. If a continuous range of resonances were available, then evidently the most strongly amplified frequency would be a continuous function of nozzle velocity. The general trend is shown by a graph of the Strouhal number, $S \equiv fD/V_0$, *vs.* the Reynolds number, $Re \equiv U_0 D/\nu$ (figure 4(*a*)). The tendency is for S to vary directly with the square root of Re according to the relation

$$S = 0{\cdot}012\sqrt{Re}. \tag{2}$$

5. The vortex-shedding frequency

The vortex-shedding frequency in the resonance régimes 1–4 was easily determined by the stroboscopic technique. In the higher régimes 5–8 it was necessary to rely on spectral analysis of the point-concentration signal produced by the scattered-light technique. The point observed (actually a $\frac{1}{2}$ mm dia. volume element) was located in the jet edge just upstream from the first ring vortex. The signal produced was a square wave with the 'on' and 'off' periods about equal. Spectra for the lower shedding frequencies exhibited a tall spike at the shedding frequency and a number of minor spikes at higher frequencies. In the resonance régimes 6–8 (embracing Reynolds numbers above 7600), however, the fundamental spike broadened into an asymmetrical hump, indicating some indeterminacy. The characteristic frequency was then taken at the maximum of the spectrum.

For the jet maximally excited by pure tones, the exciting frequency and the vortex-shedding frequency were identical in régimes 1–7. In régime 8 the exciting frequency stood at *ca.* 5700 c/s, but the shedding frequency increased with the

nozzle velocity and then levelled off at 11,000 c/s, or twice the exciting frequency. The effects of applied acoustic excitation diminished with increasing Reynolds number and became imperceptible at about $Re = 16{,}000$. The general trend of the vortex-shedding frequencies is well-described by equation (2).

Figure 4(*b*) shows two sets of data with the jet excited by intense noise (the exhaust fan). Up to $Re = 7000$ the discontinuities of the relation for pure tones are followed, but then the data fall into random scatter about the curve of equation (2).

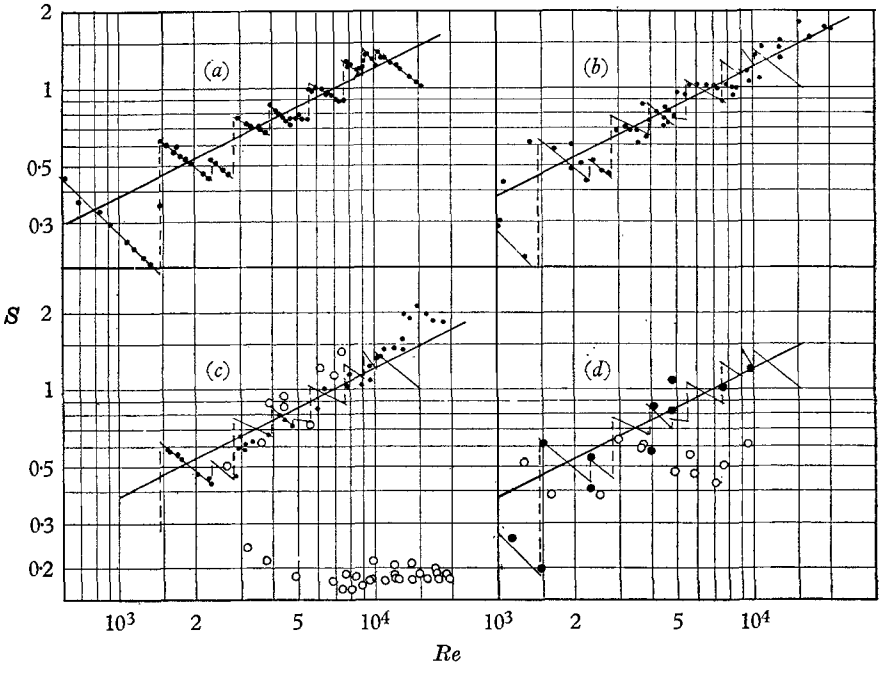

FIGURE 4. The Strouhal number $S \equiv fD/U_0$ as a function of the nozzle Reynolds number $Re \equiv U_0 D/\nu$. Graph (*a*): the tone giving maximum excitation of the free jet. Graph (*b*): the free jet vortex-shedding frequency under excitation by the noise of the exhaust fan. Graph (*c*): the free jet vortex-shedding frequency in 'silence', and (open circles) the data of Cometta (1957) on vortex shedding by spheres. Graph (*d*): the vortex-shedding frequency in confined jets at $Ct = 0{\cdot}35$ (black circles) and $Ct = 1{\cdot}22$ (open circles). The zig-zag curves in graphs (*b*), (*c*) and (*d*) are from graph (*a*). The heavy straight line in every graph is the curve of equation (2), $S = 1{\cdot}2\sqrt{Re}$.

Figure 4(*c*) shows shedding frequencies determined with minimal laboratory noise ('silence'). The discontinuous pure-tone relation is followed only up to $Re = 2800$. The hump at the highest Reynolds numbers, with a maximum at $Re = 15{,}000$, is curious but should not be taken as indicative of a continuing trend.

Figure 4(*c*) also shows the data of Cometta (1957) on eddy shedding by a sphere, with S and Re based on the sphere diameter and the free-stream velocity. At low Reynolds numbers the data on spheres 2·22, 3·79 and 5·70 cm in diameter follow the curve of equation (2). At about $Re = 7400$, the sphere Strouhal number falls abruptly to 0·19 and is thereafter independent of Reynolds

number over the remainder of the range (up to $Re = 40{,}000$) in which a periodic velocity fluctuation could be detected. For the smallest sphere tested (1·90 cm dia.) the Strouhal number was, strangely, 0·2 at Reynolds numbers below, as well as above, 7400.

It remains to mention some experiments in which the effect of an enclosure was investigated. The nozzle was mounted axisymmetrically in a 20 cm dia. duct giving $b/a = 30{\cdot}6$ for the ratio between the duct and nozzle radii. The flow pattern in such a configuration depends on the Craya–Curtet number Ct, named by Becker, Hottel & Williams (1963) for Craya & Curtet (1955) who first developed this parameter from an analysis of the mean flow. Figure 4(*d*) shows the results for two values. At $Ct = 0{\cdot}35$ the ratio of the secondary stream velocity to the nozzle velocity was 0·010, while at $Ct = 1{\cdot}22$ it was 0·038. A probably more important factor, however, is the initial value of the axial pressure gradient resulting from the gradual entrainment of the secondary stream by the jet: the initial pressure gradient at $Ct = 0{\cdot}35$ was substantially zero, while at $Ct = 1{\cdot}22$ it was large and positive, approximately $0{\cdot}06\,\rho U_0^2 a^2/b^3$. Figure 4(*d*) shows that at $Ct = 0{\cdot}35$, when the initial pressure field was like that of a free jet, the vortex-shedding frequencies followed the Strouhal number–Reynolds number relation for the free jet. At $Ct = 1{\cdot}22$, on the other hand, in the face of a fairly strong adverse pressure gradient, the Strouhal number stood substantially constant at $S = \frac{1}{2}$. It is therefore of interest that Johansen (1929) observed vortex shedding downstream of an orifice in a pipe and found the Strouhal number to be about 0·6 over the orifice Reynolds number range of 222–1020 (the ratio of pipe diameter to orifice diameter was, however, 2 compared to the present value of 30·6). We tentatively conclude that in vortex shedding by an axisymmetrial ducted jet the Strouhal number, in the event of a sufficiently strong positive pressure gradient, has a constant value of about $\frac{1}{2}$.

6. Photographic and visual observations

A photographic study of the jet in two-dimensional cross-section was made using the technique of illumination through a slit. It was also possible in the resonance régimes 1–4′ to study the vortex-shedding process visually by stroboscopic lighting.

In all régimes, axisymmetrical waves starting from the nozzle mouth were found to grow to unstable amplitude within 2–3 wavelengths distance. The wave crest slows to a standstill (indicating contact with stationary ambient air), and then folds back into the following trough. The fold then forms a ring-vortex core which rolls downstream without change in cross-sectional area. A continuous sheet of smoky air is pulled from the jet at the downstream end of the wave and winds around the rotating core interspersed with a sheet of clear ambient air drawn in at the upstream end. In other words, the waves emanating from the nozzle roll up into a succession of ring vortices. After one or two revolutions of the core, a vortex interacts strongly with the wave behind it. A variety of phenomena may then be seen. The jet excited by pure tones will be considered first.

Régime 1. $600 < Re < 1450$ (figure 5(1), plate 2)

In this low Reynolds number régime the vortices stagnate in the nascent stage; the waves fold but no rotation follows. It appears that this behaviour occurs when the potential core of the jet is shorter than about two wavelengths of the most highly amplified disturbance.

Régime 2. $1450 < Re < 2270$ (figure 2(*f*), plate 1)

The vortex cores formed by the breaking waves rotate about $\frac{1}{2}$ revolution per wavelength of translation (see also figure 6(*a*)). After the first half revolution, films and streamers of smoke shoot from the front of the vortex and form a conical shroud which is re-entrained by the jet some distance downstream (see figure 2(*e*)). At the beginning of the second revolution the vortex disintegrates into turbulent eddies.

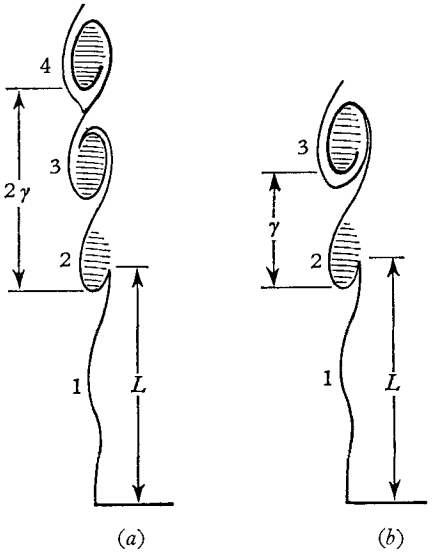

FIGURE 6. Typical patterns of disturbance evolution. In sketch (*a*) the vortex core rotates 180° per wavelength translation and in sketch (*b*), 360°.

Régime 3. $2800 < Re < 3800$ (figure 5(3), plate 2)

The angular velocity of the vortex core is about 1 revolution per wavelength of translation (see also figure 6(*b*)) and this appears to be the ultimate value, constant through this and subsequent régimes. Turbulent disintegration is preceded by a beautiful phenomenon: as seen in figure 5(3), plate 2, two large and relatively diffuse vortices appear downstream of the point at which the first revolution is completed, at intervals of double the initial wavelength. The explanation is in the fusion of vortex pairs, figure 7, plate 3. Two successive ring vortices of the initial kind interact with each other, and the trailing vortex catches up with and proceeds to thread through the larger leading one. At this point the small ring stretches and then disappears, evidently wound up on the large ring. Thereafter only the swollen large ring remains. The wavelength is

doubled, the frequency is halved, and the translational velocity remains unchanged. The enlarged vortex persists over a distance of two doubled wavelengths and bursts abruptly into turbulent eddies.

Régimes 4 *and* 4′. $3800 < Re < 7600$ (figure 5(4, 4′), plate 2)

The differences with régime 3 are small. The right-hand photograph in figure 7, plate 3, incidentally, illustrates the regularity of the vortex pattern in régimes 1–4′: while this 5 sec time-exposure was made by stroboscopic light, 5000 vortices went by.

Régime 5. $5500 < Re < 7600$ (figure 5(5), plate 2)

The initial vortices exhibit a degree of fluctuating asymmetry. The enlarged vortices resulting from fusion increased in size through régimes 3, 4 and 4′. The resultant crowding appears to have reached a limit in régime 4′; in régime 5 no increase in size is evident, but there is instead a considerable degree of chaos and a tendency toward turbulent eddying.

Régimes 6 *and* 7. $7600 < Re < 10{,}000$ (figure 5(7), plate 2)

The instability evident in régime 5 increases; the point of turbulent breakdown advances, and only a single, rather chaotically structured vortex is visible after fusion.

Régime 8. $10{,}000 < Re < 20{,}000$ (*the upper limit of this investigation*) (figure 5(8), plate 2)

The evidence of vortex fusion dissolves completely into turbulent chaos. Further, the cylindrical symmetry of the initial disturbance is gone and little or no phase-correlation is evident between waves on opposite sides of the jet. A state has been reached which will persist monotonously until (*a*) the nozzle boundary layer becomes turbulent, or (*b*) shocks appear as the Mach number becomes large. The characteristics of this state are: (i) the disturbance wavelength is very small relative to the jet diameter, (ii) the potential core persists beyond the point of onset of turbulence, and (iii) beyond the point of turbulent onset and up to the end of the potential core there exists a well-developed turbulent mixing layer.

Effects of mixed excitation

Mixed excitation containing a broad acoustic spectrum produced disturbances indistinguishable in wavelength from those by maximum excitation with pure tones. In the case of operation in 'silence', the initial disturbance amplitude was smaller and the wave-breaking point was delayed by one or two wavelengths. The angular velocity of the vortex core was a shade smaller and the first occurence of vortex fusion shifted from régime 3 to régime 4′.

Pictures with excitation by the noise of the exhaust fan were little different from those in 'silence'. In the early régimes the disturbance amplitude appeared to be intermediate between that in 'silence' and that under maximum excitation by pure tones. In régimes 6–8 all pictures were much the same regardless of how the jet was excited, save that pure tones produced greater symmetry.

7. The disturbance wavelength and the wave-breaking length

Two prominent features of the wave patterns are of interest: (i) the disturbance wavelength, λ, and (ii) the wave-breaking length, L, i.e. the distance from the nozzle mouth to the point where the waves fold or roll back. In régimes 2 and 2′ ($\frac{1}{2}$ revolution of the core per wavelength of translation) these quantities were measured as in figure 6(*a*), while in régimes 3–5 (1 revolution per wavelength) they were measured as in figure 6(*b*). In régimes 6–8 the vortices were fuzzy in appearance and the wavelength was simply measured as the average crest-to-crest distance between the visible waves.

The general trend of the wavelength and the wave-breaking length in maximum excitation by pure tones was to vary inversely as the square root of the Reynolds number:

$$\lambda/D = 43/\sqrt{Re}, \tag{3}$$

$$L/D = 107/\sqrt{Re}. \tag{4}$$

Equation (2) then indicates that $f\lambda/U_0 = \frac{1}{2}$ and $fL/U_0 = 1{\cdot}3$, if the excursions due to the resonance phenomena are smoothed out and ignored. Figure 8 shows the experimental data together with the curves of these relations.

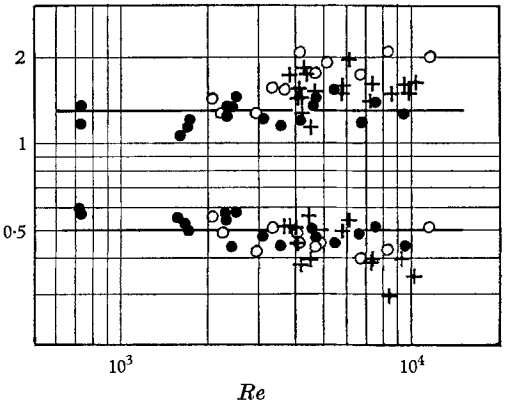

FIGURE 8. The dimensionless breaking length fL/U_0 (top curve) and the dimensionless wave velocity $f\lambda/U_0$ (bottom curve) as functions of the nozzle Reynolds number. Black circles, in maximum excitation by pure tones; open circles, in 'silence'; and crosses, in excitation by the exhaust fan.

The breaking length under maximum excitation by pure tones was constantly $2\frac{1}{2}$ wavelengths in magnitude. The interaction length (the term used by Domm *et al.* 1955)—the distance to the point of vortex fusion and wavelength doubling—was about 5 wavelengths. The turbulent disintegration length varied somewhat from one régime to the next: 6 wavelengths in régimes 2 and 2′, 9 in 3, 10 in 4 and 4′, $7\frac{1}{2}$ in 5, and 5 in 6 and subsequent régimes.

The use of mixed excitation ('silence' or intense noise) did not affect the wavelength. The breaking length L was a little longer in 'silence', reaching a maximum of 4 wavelengths.

Comparison of equations (1) and (3) shows that $\lambda/\delta = 48$, i.e. the wavelength of the disturbance with the peak growth-rate is 48 times the displacement thickness of the boundary layer at the nozzle mouth.

8. Discussion

The instability behaviour of the jet from a nozzle depends on the effluent velocity distribution. The work in this paper concerns the case of a uniform potential flow in the core with a boundary layer at the wall. In general the most highly amplified disturbance has a wavelength λ determined by the effluent boundary-layer thickness δ: λ/δ is approximately constant. The general frequency (or wave velocity) law is $f\lambda/U_0 \simeq$ const., where U_0 may be taken as the centreline velocity. When the boundary-layer thickness varies according to the thin boundary-layer law $\delta \propto \sqrt{(\nu\xi/U_0)}$ and the boundary-layer length ξ is proportional to the nozzle diameter D, then the frequency law can be stated in the form found here:

$$fD/U_0 \propto \sqrt{(U_0 D/\nu)}.$$

When, on the other hand, the laminar boundary-layer completely fills the nozzle, δ/D is a constant, λ/D is a constant, and the frequency law can be stated as $fD/U_0 =$ const. The transition between these régimes takes place in a critical range of $\delta/D \propto \sqrt{(\nu\xi/D^2U_0)}$ around $\nu\xi/D^2U_0 = 0{\cdot}01$. Sato (1960) observed both régimes in planosymmetrical jets. It should be noted that while the thin boundary-layer régime gives varicose instability, the full boundary-layer régime usually leads to sinuous instability. Thus the difference goes beyond merely a change in the frequency law.

It follows that the jet formed by Poisieulle flow from a tube belongs to the full boundary-layer case and should exhibit sinuous instability.

The jet from a square-edged orifice plate, however, is a case by itself. In the flow through the orifice there should be an eddying in the space between the shoulder and the separating flow rounding the shoulder. The eddy would be proportional in size to the orifice thickness t and might determine the effective shear layer thickness δ at the start of the jet and hence the disturbance wavelength λ. An evolution along such lines is suggested by the results of Anderson (1956) which indicate the frequency law $ft/U_0 =$ const. in the orifice Reynolds number range 2000–10,000.

The sharp-edged (knife-edged) orifice is another case. Here the boundary layer developed along the inside surface of the orifice plate may be decisive, however great the pinch at the orifice edge. Wehrmann, Fabian & Wille (1956) found the frequency law to be $fD/U_0 \propto \sqrt{(U_0 D/\nu)}$ in the orifice Reynolds number range of 6000 to 30,000, a result indicative of the thin boundary-layer case.

The phenomena associated with orifices have been only fragmentarily observed and more work is needed to obtain clarification. The behaviour of jets issuing from long tubes also needs further study.

The coincidence between the frequency law of our jet and Cometta's results on spheres (figure 4(*c*)), is explained in part by the general hypothesis that the disturbance with maximum growth is determined by the initial thickness of the free shear layer. The displacement thickness of the sphere boundary-layer at separation is (Schlichting 1962) $\delta/D \simeq 1/\sqrt{Re}$, similar to our equation (1). The near coincidence of the critical Reynolds number of about 7600 for the

onset of spottiness in the disturbance pattern of the jet and the Reynolds number of 7400 for the abrupt drop in the sphere Strouhal number to 0·19 appears significant. Perhaps the varicose mode of instability in the sphere wake breaks down at this point and gives way to a sinuous disturbance with wavelength long relative to, and in a constant ratio with, the sphere diameter.

The present work could not be carried to Reynolds numbers above 20,000. However, Kolpin (1964) has made shadowgraphs of jets from 1·27 cm and 2.54 cm dia. nozzles and these show wave patterns similar to those at our highest Reynolds numbers. Measurements on the published pictures give $\lambda/D = 46/\sqrt{Re}$ and $L = 3{\cdot}3\lambda$ for Reynolds numbers between 6×10^4 and 6×10^5. This result for the wavelength agrees closely with ours, equation (3). The breaking length is comparable to our result for 'silence', the condition most similar to Kolpin's.

Domm *et al.* (1955) and Wehrmann *et al.* (1956) experimented with circularly faired flow nozzles on which the fairing radius equalled the throat diameter. For throat diameters from 1 to 10 cm the frequency law was

$$fD/U_0 = 0{\cdot}0122\sqrt{Re},$$

which agrees with our result, equation (2). Later Michalke designed a 'vortex filament' nozzle on which the boundary-layer displacement thickness is easily calculated; at exit $\delta/D = 1{\cdot}2/\sqrt{Re}$. Experiments with different nozzle diameters all gave $f\delta/U_0 = 0{\cdot}0234$ for the most strongly amplified disturbance (Schade & Michalke 1962). The frequency law from these data is

$$fD/U_0 = 0{\cdot}0195\sqrt{Re},$$

in which the constant differs significantly from the above results and ours. These values perhaps indicate the range of variation due to nozzle design. The present work was carried out with a single nozzle diameter. However, the results cited in the preceding paragraph, covering a tenfold range in nozzle diameters and two nozzle geometries, sufficiently prove the validity of our generalizations under this test.

The theoretical value of the dimensionless wave velocity $f\lambda/U_0$ for varicose disturbance of a cylindrical vortex sheet with λ not large relative to the diameter is $\frac{1}{2}$ (Batchelor & Gill 1962; Schade & Michalke 1962). Our results (figure 8), agree. Those of Schade & Michalke indicate a value of 0·59. Anderson (1956) found 0·53.

Simple inviscid instability theory based on the Rayleigh straight-line approximations to the shear layer velocity distribution gives $\lambda/\delta = 23{\cdot}7$ for the ratio between the wavelength of the most strongly amplified disturbance and the boundary-layer thickness at the nozzle exit (Schade & Michalke 1962). The data of Schade & Michalke on the vortex filament nozzles give 25·1. Ours give 48. A study aimed at finding and explaining the range of variation of λ/δ may be desirable.

The discrete resonance frequencies found in our work, giving a discontinuous relation between the frequency of the most highly amplified disturbance and the nozzle velocity, appear to be due to resonances of the nozzle chamber. We have not had the opportunity to investigate the matter further with our original

apparatus, and in this paper we have emphasized the continuous and universal trend of the results rather than the discontinuous and peculiar.

The sensitivity of our jet to applied acoustic excitation was most acute at nozzle Reynolds numbers below 7600, or boundary-layer Reynolds numbers $\delta U_0/\nu$ below 80. At higher Reynolds numbers the disturbance pattern fell into spottiness and the response became very much weaker.

Resonance tones and jet tones have been systematically studied by Anderson (1954, 1955, 1956), but only in the case of jets from square-edged orifices. Andrade (1941) found that selective acoustic sensitivity in sinuous instability is due to transverse vibrations of the nozzle forced by the natural modes of vibration of whatever gear the nozzle is mechanically coupled with. A conclusive investigation for thin-boundary layer jets is so far lacking. Indeed the present investigation appears to be the first to have encountered the phenomena in this case.

This work was supported by the U.S. Army Research Office (Durham); Grant no. DA-ARO (D)-31-124-68 and Project no. 2013-E. The experiments were done in the Fuels Research Laboratory, Department of Chemical Engineering, Massachusetts Institute of Technology, Cambridge, Massachussetts. A part of the work was used in the B.Sc. thesis of one of the authors (T. A. M.) at M.I.T.

REFERENCES

ANDERSON, A. B. C. 1954 *J. Acoust. Soc. Am.* **26**, 21.

ANDERSON, A. B. C. 1955 *J. Acoust. Soc. Am.* **27**, 1048.

ANDERSON, A. B. C. 1956 *J. Acoust. Soc. Am.* **28**, 914.

ANDRADE, E. N. da C. 1941 *Proc. Phys. Soc.* **53**, 329.

BATCHELOR, G. K. & GILL, A. E. 1962 *J. Fluid Mech.* **14**, 529.

BECKER, H. A., HOTTEL, H. C. & WILLIAMS, G. C. 1963 *Ninth Symposium (International) on Combustion*, p. 7.

BECKER, H. A., HOTTEL, H. C. & WILLIAMS, G. C. 1967 On the light-scatter technique for the study of turbulence and mixing. *J. Fluid Mech.* **30**, 259.

COMETTA, C. 1957 An investigation of the unsteady flow patterns in the wake of cylinders and spheres using a hot-wire probe. *Technical Note* no. AFOSR-TN-57-760. *Document*, no. AD 136749: U.S. Air Force Office of Scientific Research.

CRAYA, A. & CURTET, R. 1955 *C.r. hebd. Seanc. Acad. Sci., Paris* **241**, 621.

DOMM, U., FABIAN, H., WEHRMANN, O & WILLE, R. 1955 Contributions on the mechanics of laminar-turbulent transition of jet flow. Air Force Office of Scientific Research. *Techt. Rept.* (AFOSR TR), 56–9; Armed Forces Technical Information Agency (ASTIA), *Document*, no. AD 82004.

DOMM, U. 1956 Über eine Hypothese, die den Mechanisms der Turbulenz-Entstehung betrifft. *DVL Bericht* no. 23.

JOHANSEN, F. C. 1929 *Proc. Roy. Soc.* A**126**, 231.

KOLPIN, M. A. 1964 *J. Fluid Mech.* **18**, 529.

LECONTE, J. 1858 *Phil. Mag.* **15**, 235.

MICHALKE, A. 1964 *Ingenieur Archiv*, **33**, 264; *J. Fluid Mech.* **19**, 543.

MICHALKE, A. & SCHADE, A. 1963 *Ingenieur Archiv.* **33**, 1.

RAYLEIGH, LORD 1879 *Phil. Mag.* **15**, 235 (also *Scientific Papers*, Art. 61).

RAYLEIGH, LORD 1884 *Phil. Mag.* **17**, 188 (also *Scientific Papers*, Art. 110).

RAYLEIGH, LORD 1899 *Scientific Papers*, Arts. 58, 60 and 66. Cambridge University Press.

SATO, H. 1960 *J. Fluid Mech.* **7**, 53.

SCHADE, H. 1964 *Phys. Fluids*, **7**, 623.

SCHADE, H. & MICHALKE, A. 1962 *Z. Flugwissenschaft*, **10**, 147.

SCHLICHTING, H. 1962 *Boundary Layer Theory* (fourth edition). New York: McGraw-Hill.

WEHRMANN, O., FABIAN, H. & WILLE, R. 1956 Further investigations of the laminar-turbulent transition in a free jet (annular nozzle). Air Force Office of Scientific Research. *Tech. Rept.* (AFOSR TR), 57–31; Armed Forces Technical Information Agency (ASTIA), *Document*, no. AS 126494.

WEHRMANN, O. & WILLE, R. 1957 *Proc. Boundary Layer Symposium*, Freiburg, p. 387.

WILLE, R. 1963 Growth of velocity fluctuations leading to turbulence in free shear flow. *Tech. Rept.* Hermann Föttinger Institut für Strömungstechnik an der Technischen Universität Berlin.

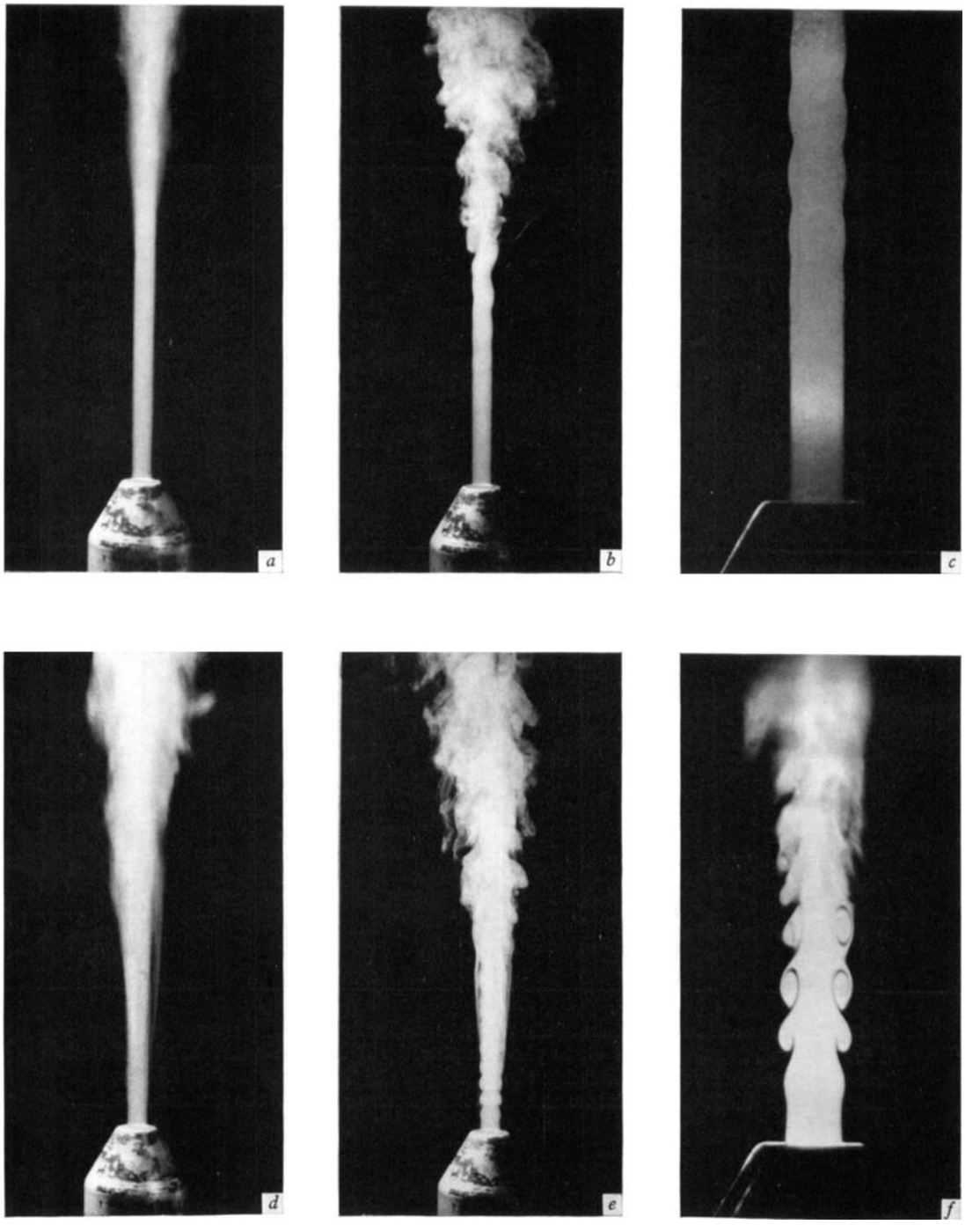

FIGURE 2. The jet at a Reynolds number of 1690. (*a*), (*b*) and (*c*) show the jet in 'silence'. while (*d*), (*e*) and (*f*) show it excited by the pure tone, 370 c/s, giving maximum response. (*a*) and (*d*) are $\frac{1}{25}$ sec exposures. (*b*), (*c*) and (*e*) are 'instantaneous' flash exposures, *f* is a 5 sec time exposure by stroboscopic light. (*a*), (*b*), (*d*) and (*e*) were taken by strong general illumination, while the close ups (*c*) and (*f*) were taken by illumination through a slit and show a longitudinal cross-section of the jet.

BECKER AND MASSARO (*Facing p.* 448)

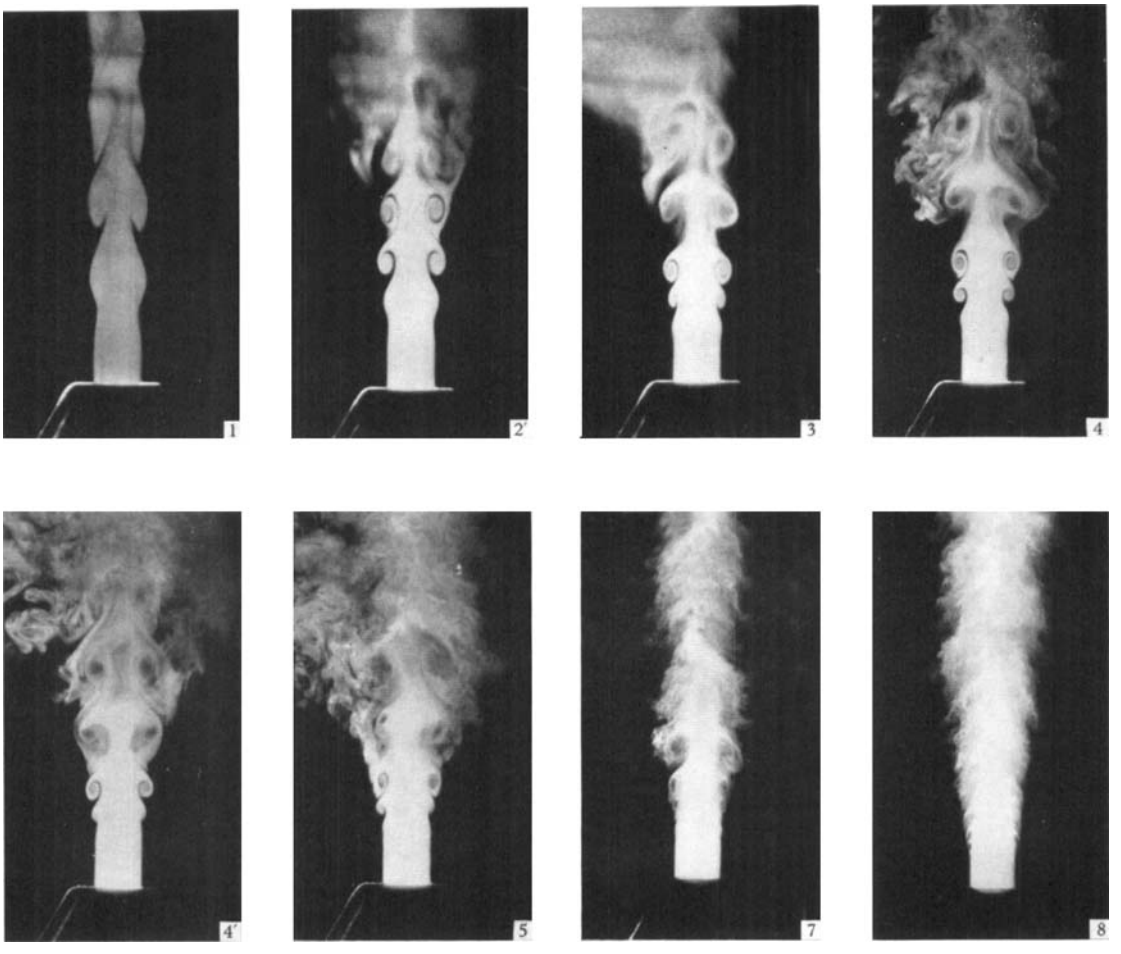

FIGURE 5. The resonance régimes of the free jet maximally excited by pure tones as seen in longitudinal cross-sectional views photographed by light from a slit. 1, 2′ and 3 are time exposures by stroboscopic light ; the remainder are 'instantaneous' flash exposures. See table 1 for the frequency values and Reynolds number ranges of the resonance régimes.

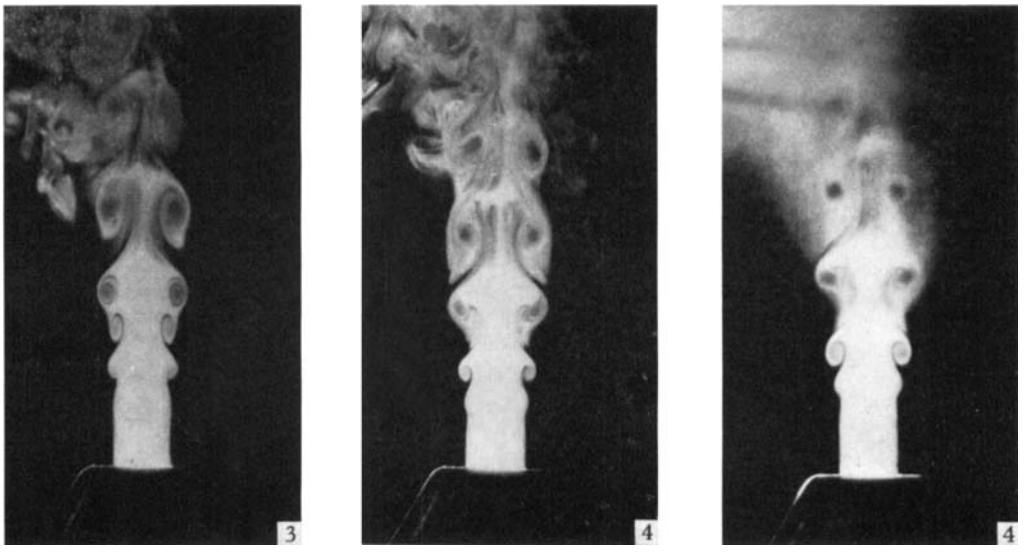

FIGURE 7. Photographs illustrating the process of vortex fusion.